Aerosol and Air Quality Research, x: 1–11, xxxx

ISSN: 1680-8584 print / 2071-1409 online
doi: 10.4209/aaqr.2018.07.0269

Insights into the Effect of Adsorption-Desorption Cycles on SO_2 Removal over an Activated Carbon

Shaojun Liu[1,2], Xinning Yu[1], Guoxin Lin[1], Ruiyang Qu[1], Chenghang Zheng[1], Xiang Gao[1*]

[1] *State Key Laboratory of Clean Energy Utilization, Zhejiang University, Hangzhou 310027, China*
[2] *Key Laboratory of Low-grade Energy Utilization Technologies and Systems of the Ministry of Education of China, College of Power Engineering, Chongqing University, Chongqing 400030,China*

ABSTRACT

The use of an activated carbon (AC) with high ash content (15.92%) for SO_2 removal was investigated during adsorption-desorption cycles. Significant deterioration in both dynamic and equilibria adsorption processes during the cycles was observed. To investigate the causes of deactivation, SO_2 temperature-programmed desorption (SO_2-TPD) experiments were conducted. The results indicated that most of the stored sulfur-containing species were released in the form of SO_2 when the temperature was below 400°C. In addition to SO_2, traces of CO were detected, but higher temperatures were required for the abundant release of CO. A Fourier-transform infrared spectrometry (FTIR) experiment was used to investigate changes in the oxygen-containing groups, and the results confirmed the formation of stable C-O complexes. These formations were tentatively attributed to the CO precursor's occupation of active sites. Based on the formation of C-O complexes, two deactivation pathways in the cycles were proposed. The adsorption-desorption cycles also affected the AC ash. The formation of sulfur-containing species in the ash was confirmed through thermodynamic calculation and powder X-ray diffraction.

Keywords: Activated carbon; Adsorption; Desorption; SO_2 removal.

INTRODUCTION

SO_2 resulting from fossil fuel combustion is a major source of air pollution, which contributes to the formation of acid rain. Several methods have been used commercially for the reduction of SO_2 emissions, such as wet flue gas desulfurization (WFGD), semidry flue gas desulfurization (semidry FGD), and dry flue gas desulfurization (dry FGD; Wang *et al*., 2017; Ni *et al*., 2018). The activated carbon (AC)-based desulfurization process is categorized as dry FGD, which has attracted research attention because of its potential for use in converting SO_2 into by-products of higher value, such as H_2SO_4 or S. Moreover, this process requires relatively little or even no water, in contrast to conventional WFGD or semidry FGD; thus, it is a suitable process for water-deficient areas (Gao *et al*., 2011a; Guo *et al*., 2015; Li *et al*., 2016).

The following reactions govern the desulfurization process (Rosas *et al*., 2017):

$$SO_2 + \frac{1}{2}O_2 \rightarrow SO_3 \quad (1)$$

$$SO_3 + H_2O \rightarrow H_2SO_4 \quad (2)$$

These reactions may occur at different locations and be influenced by various properties of AC. It is generally accepted that oxidation of SO_2 is limited to the vicinity of active sites, and hydration of SO_3 usually occurs within the pores of AC, which offer a relatively large amount of space for reaction (Mochida *et al*., 1997; Ma *et al*., 2003; Gaur *et al*., 2006; Sun *et al*., 2015). Further research should be conducted to identify the active sites in SO_2 oxidation. Although Zhang *et al*. posited that C-O-C in ethers and C=O in quinones are the main active sites (Zhang *et al*., 2017), most researchers have inferred that bare carbon atoms located in edge positions are responsible for SO_2 adsorption (Lizzio and DeBarr, 1996; Mochida *et al*., 1997; Mochida *et al*., 1999; Yang and Yang, 2003; Liu *et al*., 2016; Sun *et al*., 2016). Regarding hydration of SO_3, the pore structure of AC may play a critical role, details about which have been reported based on a rigorous, long-term study. Initially, Lizzio and DeBarr (1996) demonstrated that SO_2 adsorption does not exhibit a relationship with a specific area of AC, whereas Rubio and Izquierdo (1997)

* Corresponding author.
Tel.: 1-350-571-1887; Fax: 0571-87951335
E-mail address: xgao1@zju.edu.cn

and Rubio *et al*. (1998) suggested that optimizing the surface area could promote SO_2 adsorption. Until very recently, hierarchical structures, such as micro-, meso- and macropores, could be classified (Gao *et al*., 2011b; Yu *et al*., 2018). Based on these preliminary findings, Sun *et al*. (2015) suggested that meso- and macropores serve in H_2SO_4 transportation, facilitating the overall process. Researchers have also discovered a linear relationship between SO_2 uptake and volumes of ultramicropores on special CO_2-activated carbons (Zhu *et al*., 2012).

Besides these findings, more complex topics are the roles of AC chemical properties in SO_2 removal. The basicity of a surface may be assumed to promote adsorption of acidic SO_2 (Atanes *et al*., 2012; Zhu *et al*., 2012; Ren *et al*., 2017). However, a promotion effect from acidic oxygen-containing groups such as carboxyl groups has also been reported (Liu *et al*., 2016; Cui *et al*., 2017).

Desulfurization is a continuous process, and ACs are degraded in adsorption-desorption cycles, which cause changes in their physical and chemical properties; these changes, in turn, affect SO_2 removal. Additionally, the cost of an AC is a critical concern for process commercialization (Mochida *et al*., 2000). In previous studies, cheap precursors, such as low-grade coals, have been used for AC preparation, resulting in considerable amounts of ash in the ACs (Lizzio and DeBarr, 1996; DeBarr *et al*., 1997; Rubio and Izquierdo, 1997, 1998; Rubio *et al*., 1998; Izquierdo *et al*., 2003; Liu *et al*., 2003a; Liu *et al*., 2003b). However, to the best of our knowledge, few studies have discussed the conversion of ash in the AC desulfurization process.

This investigation focused on the physical and chemical changes of AC during adsorption-desorption cycles. Specifically, variations of texture, oxygen-containing groups, and ash were evaluated. The findings revealed the effects of adsorption-desorption cycles on SO_2 removal.

METHODS

Preparation of the Activated Carbon

Commercial AC obtained from Xinhua Chemical Company (Taiyuan, China) was used as the precursor in this study. The results of elemental and proximate analyses of the as-received carbon are presented in Table 1. To evaluate the effect of adsorption-desorption cycles, the as-received carbon was treated using various cycle times. The nomenclature of each sample included the precursor (A), treatment method (R), and times. The following sample was also prepared for comparison: A-H10 (treated under nitrogen at 400°C for 10 h).

Activity Tests of the Activated Carbon

All of the tests were performed in an experimental installation constructed for this study (Fig. 1). The activities of SO_2 removal were investigated using various procedures, described as follows: (i) In dynamic tests, the feed gas was passed through the fixed bed at a constant temperature. Concentrations of SO_2 and O_2 in the inlet and the outlet of the reactor were measured online using a flue gas analyzer (Testo 350, Germany). Measurements were stopped at a breakthrough concentration of 4000 ppm. (ii) In equilibria tests, a flow was admitted into the reactor for 1 h, and the samples were then heated at 10°C min^{-1} under a flow of N_2 up to 400°C and maintained for 1 h. Adsorbed and desorbed SO_2 were detected using a slightly modified version of the procedure proposed by Davini (2001). After passing through the reactor, the adsorbed or desorbed gas flowed through a scrubbing bottle that contained 250 mL of hydrogen peroxide (5 vol.%). The effluent gases were assumed to contain SO_x (SO_2 and SO_3), CO, CO_2, N_2, and O_2, among which only SO_x and CO_2 could be trapped by the H_2O_2 solution and converted to H_2SO_4 and H_2CO_3, respectively. The reacted solution was separated into two parts: The first part was titrated using a 0.01 M NaOH solution, and the second part was diluted and then evaluated using ion chromatography (792 Basic IC, Metrohm, Switzerland). These two evaluation methods guaranteed the validity of the results. The experimental error is discussed in a later section. The amount of adsorbed SO_2 was determined based on the difference between the results without and with carbon.

For all of the adsorption processes, the gaseous mixture was 1 vol.% SO_2, 7 vol.% O_2, and 12 vol.% H_2O in N_2 and at 120°C before the AC bed was introduced. Water vapor was fed by means of a saturator through which part of the mixture bubbled before entering the reactor. The amount of vapor fed was controlled by the temperature of the bath in which the saturator is immersed, assuming vapor–liquid equilibrium followed Antoine's law. The loaded ACs were cylindrical particles with a 5 mm diameter. The total flow rate of the mixture was maintained at 1.1 L min^{-1} using flow meters, resulting in a space velocity of 800 h^{-1}. Consecutive adsorption-desorption cycles were performed, and the characteristics of the samples were assessed at the end of the cyclic processes.

Characterization of the Activated Carbon

N_2 adsorption was performed at 77 K using an Autosorb-1-C installment (Quantachrome Instruments). The specific surface areas were calculated employing the Brunauer-Emmeet-Teller (BET) equation, while the total pore volumes and micropore volumes were decided by single point adsorption quantity at $P/P_0 = 0.95$ and *t*-plot method, respectively. Prior to the N_2 sorption, the sample was preheated at 250°C for about 3 h to remove physically sorbed material from narrow pores.

Table 1. Elemental and proximate analyses of the as-received carbon.

Material	Elemental analysis (%, wt.)					Proximate analysis (%, wt.)			
	C	H	O[a]	N	S	Moisture	Ash	Volatile	Fixed carbon
A-R0	69.07	1.60	3.22	0.4	0.5	9.29	15.92	3.71	71.08

[a] By difference.

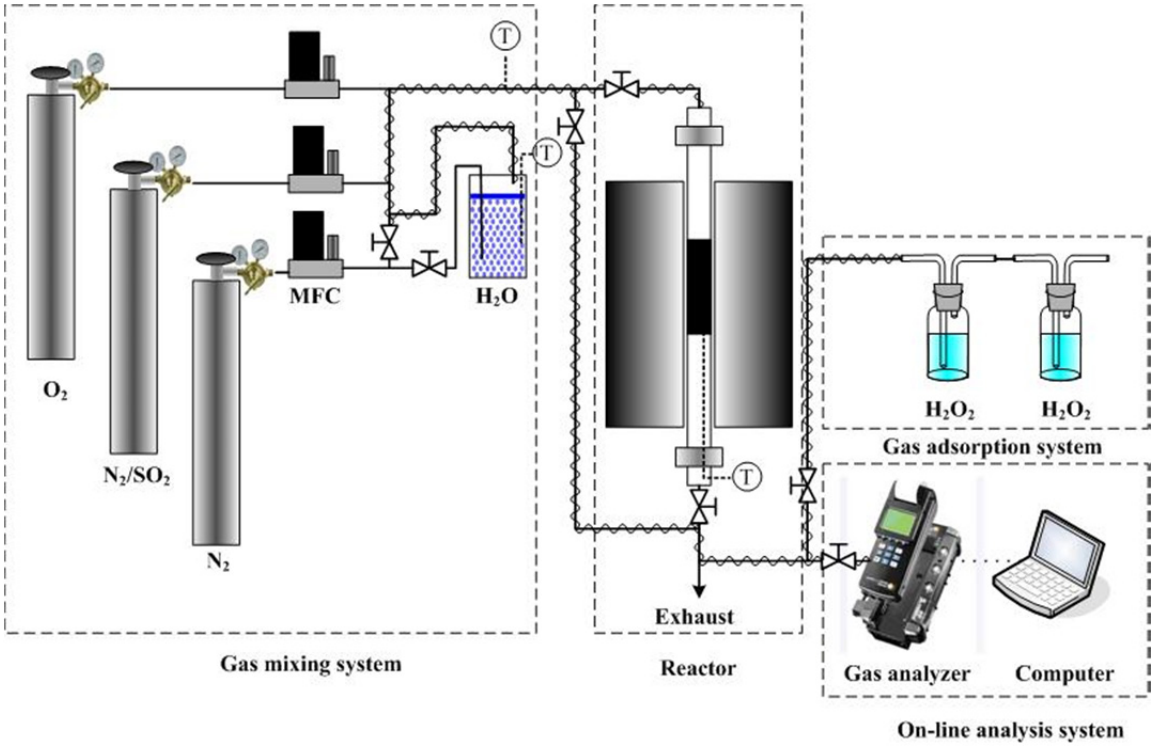

Fig. 1. Experimental installation for SO_2 experiments (MFC, mass flow controller; T, temperature controller).

Temperature-programmed desorption (TPD) experiments were carried out in the same apparatus as the activity test. In a typical run, a sample was heated under a flow of N_2 (1.1 L min^{-1}) from room temperature to 750°C at a rate of 5°C min^{-1} to achieve nearly complete desorption of SO_2. During the desorption, traces of SO_2 and CO were monitored.

Fourier-transform infrared spectrometry (FTIR) tests were carried out on a Nicolet 380 Spectrometer (Thermo Electron) at ambient temperature. The samples were mixed with KBr at a mass ratio of 1:100, grounded and then pressed into a thin slice. Thirty-two scans were made to yield a spectrum with a resolution of 4 cm^{-1} spanning 400–4000 cm^{-1}.

Powder X-ray diffraction (XRD) patterns were collected with an X'Pert PRO diffractometer using a Cu Kα radiation source. X-ray photoelectron spectroscopy (XPS) spectra were obtained with a Thermo ESCALAB 250Xi using Al Kα X-ray source (hν = 1486.6 eV). The C_{1s} spectrum peaked at 284.8 eV was taken as the reference. The pH_{pzc} values of carbon were determined by contacting 0.15 g of the sample with 2 mL distilled water for 3 days. It has been confirmed that in this case the pH value of solution was equal to the pH_{pzc} value of carbon (Lizzio and DeBarr, 1996; Martin *et al*., 2002).

The ash composition of the as-received carbon was detected using an X-ray fluorescence (XRF) method in a Rigaku ZSX100e.

Thermodynamic Calculations

For the analysis, mineral impurity in AC was considered. Gaseous SO_2, H_2O and O_2 as well as the solid mineral and carbon were regarded as reactants in the process of adsorption at 120°C, while H_2SO_4 instead of gaseous components was involved in the process of desorption at 400°C. The software package FactSage version 5.2 was used for the thermodynamic calculations.

RESULTS AND DISCUSSION

Dynamic Tests

Changes in the SO_2 adsorption profiles for various samples are denoted in Fig. 2. For sample A-R2, little change was observed. However, with the increase in the number of cycles, the slopes of the profiles became steeper. Thus, for sample A-R10, the outlet SO_2 concentration reached approximately 38% of the amount at the inlet within 12 min, which can be compared with the 30 min required for the original AC (A-R0).

Equilibria Tests

Fig. 3 indicates the amounts of sulfur dioxide that were adsorbed and desorbed over several consecutive cycles. As mentioned, ion chromatography and acid-base titration were used for mutual verification. During the adsorption process, two broad peaks were evident. The uptake amount increased up to two cycles and decreased to a lower value after four cycles. Subsequently, after a slight ascent, the amount gradually decreased after six cycles. The amounts detected using the two methods were in good agreement, implying that the results were accurate. A clear reduction in SO_2 adsorption was observed. After 10 cycles, 15% loss was confirmed according to the ion chromatography method, and acid-base titration method indicated 10% loss. Regarding desorption, similar features were observed, and

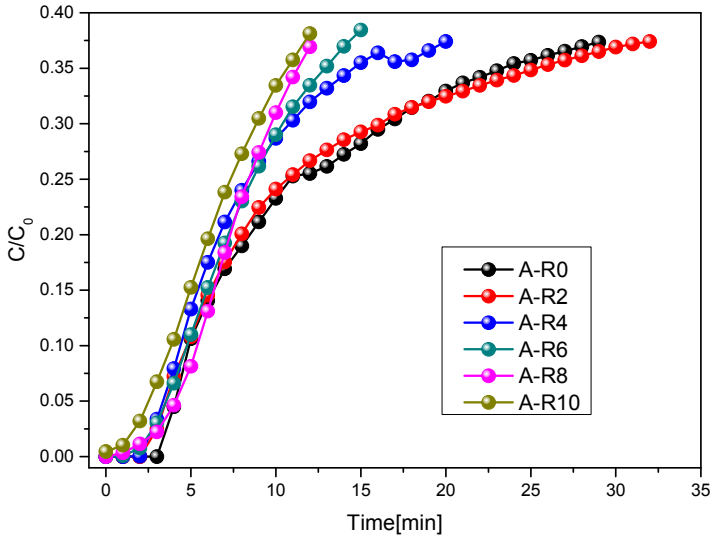

Fig. 2. Dynamic tests for SO_2 adsorption in samples with various cycles. Adsorption conditions: 1 vol.% SO_2, 7 vol.% O_2, 12 vol.% H_2O, 120°C, 800 h^{-1}. Desorption conditions: 400°C in N_2 for 1 h, 800 h^{-1}.

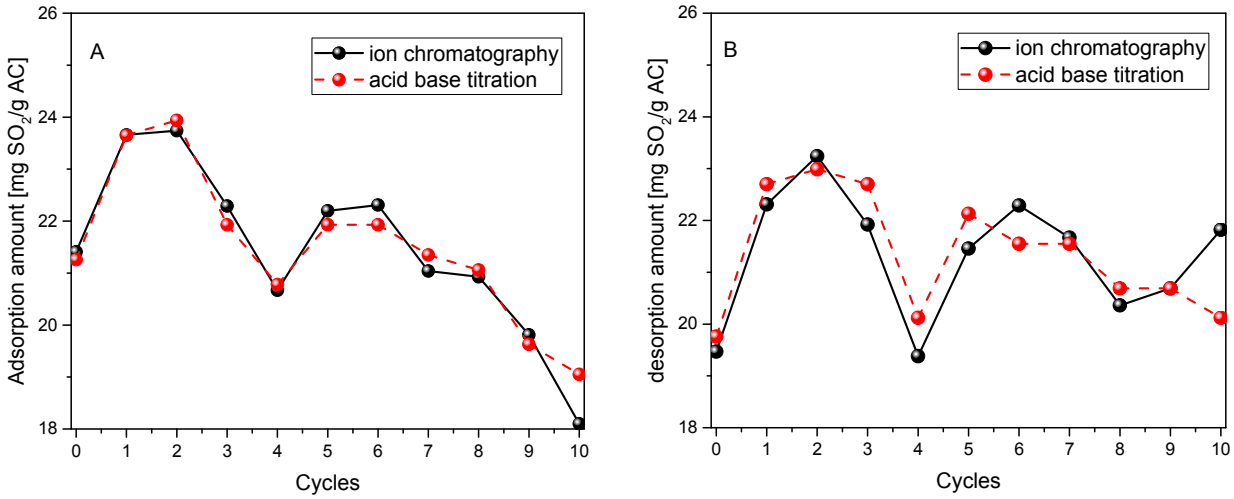

Fig. 3. SO_2 adsorption and desorption amounts for various cycles. Adsorption conditions: 1 vol.% SO_2, 7 vol.% O_2, 12 vol.% H_2O, 120 °C, 800 h^{-1} for 1 h. Desorption conditions: 400°C in N_2 for 1 h, 800 h^{-1}.

two broad peaks were clear. However, compared with the descending trend in the adsorption results, the desorption data notably fluctuated at approximately 21 mg SO_2 g^{-1} AC. Additionally, a small difference between the amounts detected using the two methods was observed. This difference was attributed to the measurement principle. For the ion chromatograph, only SO_4^{2-} in solution was included in calculations of SO_2 amount, whereas in cases of acid-base titration, H^+ derived from both H_2SO_4 and H_2CO_3 in solution was used in the calculations. Consequently, during the desorption process, release of CO_2 from the AC may have affected calculation of SO_2 desorption amount in cases of acid-base titration. However, although differences between the results from the two methods were observed in each adsorption-desorption cycle, the ratios of average desorption amount to average adsorption amount were the same, at 99.4%. Thus, the diminishment of desulfurization may have been partially due to the residual SO_2 from previous cycles.

SO_2-TPD

SO_2-TPD experiments were conducted to further investigate the causes of deactivation. Fig. 4 illustrates the TPD profiles of SO_2 based on desorption of saturated Sample A-R0.

All of the SO_2-TPD profiles exhibited desorption peaks at approximately 330°C. The TPD profile of SO_2 adsorbed with 12% H_2O exhibited the least amount of desorption; the amount was even less than the amount desorbed under the condition of SO_2 adsorbed alone. This phenomenon clearly indicated that competitive adsorption between SO_2 and H_2O occurred on the sample surface, as suggested by Liu *et al*. (2003b). The amount desorbed increased with the introduction of O_2. At 330°C, two nearly coincident peaks

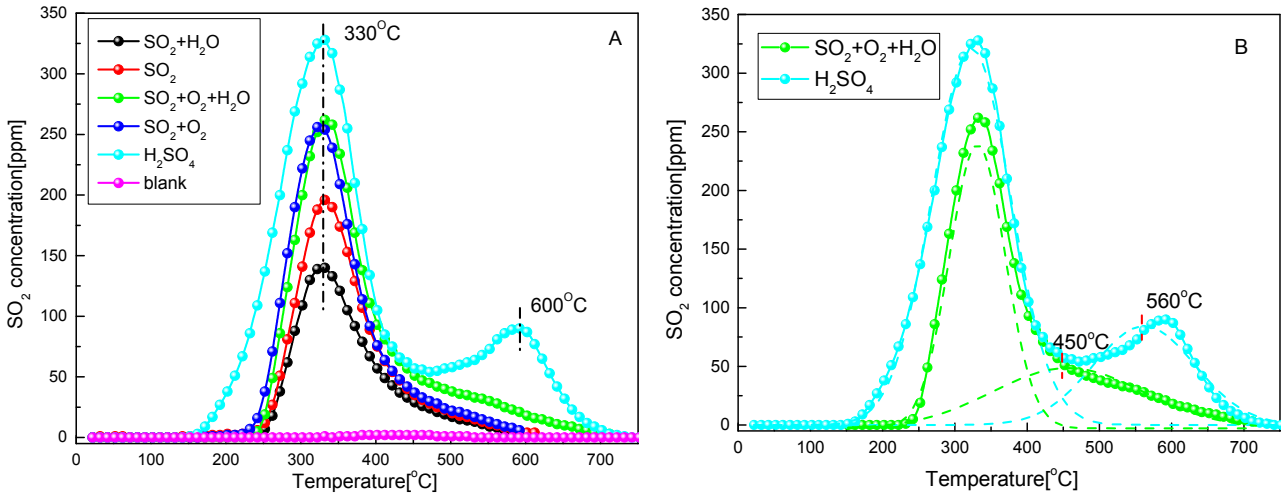

Fig. 4. TPD profiles of SO_2 from AC after adsorption tests. (a) Effect of pretreatment and (b) deconvolution results.

were observed for profiles of SO_2 adsorbed with O_2 and SO_2 adsorbed with O_2 and H_2O. However, the TPD profile of SO_2 adsorbed with O_2 and H_2O exhibited a shoulder peak at the higher temperature. Mochida *et al*. (1999) suggested that H_2O increased SO_2 adsorption through oxidation and hydration of adsorbed SO_2, resulting in the formation of adsorbed H_2SO_4. The profile of sample A-R0 impregnated with H_2SO_4 exhibited two desorption peaks, one at 330°C and the other at 600°C, corresponding with the main peak and the shoulder peak under the condition of SO_2 adsorbed with O_2 and H_2O. Therefore, two types of sulfur-containing species were inferred to have existed on the carbon surface. One part may have been adsorbed on the active sites of the carbon with strength equal to the adsorbed SO_2. The others may have been stored in the pores of the carbon due to the elution effect of the water. The results may also be partly ascribed to sulfates, which are described in a later section.

Fig. 5 illustrates the TPD profiles of CO that accompanied SO_2 desorption. A blank sample without any adsorption was used as a reference. CO desorption increased rapidly at higher temperatures (> 400°C). At lower temperatures (250–400°C), minor peaks for SO_2 adsorbed with O_2 and H_2O as well as Sample A-R0 impregnated with H_2SO_4 were observed. This temperature window corresponded with that of the main SO_2 desorption peak. These findings may be interpreted in terms of the temperature programmed superficial reaction described by Perrard and Joly (1989). According to the proposed mechanism, the large amounts of CO observed after SO_2 adsorption demonstrated that carbon was oxidized during TPD (Martin *et al*., 2002). The oxidizing agent was SO_3 derived from the decomposition of H_2SO_4. The reducing agent was carbon, and as a consequence of oxidation reactions, oxygen-containing groups formed, and SO_2 was released (Muniz *et al*., 1998). The oxygen-containing groups could then be thermally decomposed into CO or CO_2 at different temperatures depending on the group type. A minor evolution of CO occurred from 250 to 400°C as a result of unstable groups. A substantial increase in the amount of evolved CO at higher temperatures was caused by the decomposition of stable groups. Because the regeneration temperature was 400°C (Figs. 2 and 3), the CO-forming groups likely formed through a superficial reaction and remained on the AC surface until they reached their natural decomposition temperatures. Compared with the sample impregnated with H_2SO_4, the sample pretreated with $SO_2 + O_2 + H_2O$ released more CO between 500 and 650°C. This phenomenon may have resulted from the increase in unstable CO-forming groups produced in the reaction between carbon and H_2SO_4. These findings were consistent with the previous SO_2-TPD results (Fig. 4(a)), which revealed two peaks over both the $SO_2 + O_2 + H_2O$ pretreated and H_2SO_4 impregnated samples. After deconvolution using the Gaussian function, it is clear to see that the second peak of SO_2 shifted to a lower temperature over the $SO_2 + O_2 + H_2O$ pretreated sample (Fig. 4(b)), and this result agreed well with the increase in CO release between 500 and 650°C.

Characterization Results

The textural characteristics of the samples were investigated, and the results are presented in Table 2. Compared with those of the original AC, the BET surface area (S_{N_2}), total pore volume (V_p) and micropore volume (V_{micro}) increased after the cycles, whereas average pore diameter (D_{avg}) decreased. Note that after 10 cycles, the ratio of V_{micro}/V_p dropped from 0.47 to 0.36, indicating a relative reduction of micropore volumes, which play an important role in SO_2 adsorption. The changes in textural properties were mostly caused by the increasing degree of burn-off. However, the textural changes were difficult to correlate with the results of the dynamic or equilibria tests because of the generally accepted proposal that well-developed pore structures prompt adsorption.

A more precise understanding of SO_2 adsorption behavior may require more detailed information about the oxygen-containing groups formed after adsorption-desorption cycles. A Fourier-transform infrared spectroscopy (FTIR) experiment was used to investigate changes of the oxygen-containing groups. In general, CO_2 is derived from acidic surface oxides, such as carboxyl and lactone groups, and

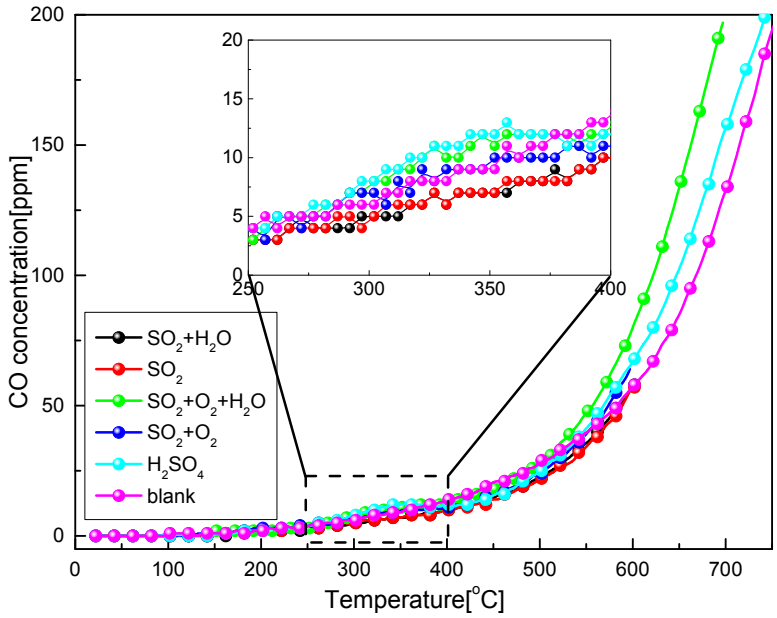

Fig. 5. TPD profiles of CO from AC after adsorption tests.

Table 2. Textural and acid-base characterization of the samples.

Sample	S_{N_2} (m^2 g^{-1})	V_p (cm^3 g^{-1})	V_{micro} (cm^3 g^{-1})	D_{avg} (nm)	pH_{pzc}
AC-R0	101	0.1090	0.0515	4.307	8.70
AC-R1	179	0.1374	--	3.073	8.94
AC-R2	156	0.1419	--	3.637	9.04
AC-R3	182	0.1346	--	2.957	9.13
AC-R10	206	0.2067	0.0745	4.021	--

CO is produced by ketone, aldehyde, and phenol, which are basic surface oxides (Muniz *et al*., 1998; Mochida *et al*., 2000). In the recorded spectra (Fig.6), the absorption band in the 3000–2700 cm^{-1} range could be assigned to the stretching vibrations of C-H in aldehyde. Bands at 2854 cm^{-1} and 2926 cm^{-1} were detected in the cases of A-R1 and A-R2, indicating that some aldehyde groups had appeared on the surface of the carbon. The presence of bands between 1200 cm^{-1} and 1000 cm^{-1} may have been caused by vibration of C-O in phenol (Shin *et al*., 1997). The peak at 1084 cm^{-1} considerably increased after the cycles, implying an increase in phenol groups.

Based on these findings, the surface basicity of the sample should have been higher after the cycles. This deduction was confirmed through investigation of the pH_{pzc} values of the carbons, as presented in Table 2. The point of zero charge was defined as the pH where the net surface charge resulting from the adsorption of the potential-determining ions, H^+ and OH^-, was zero. In aqueous solution, Brønsted acidic groups of the carbon surface tended to donate their protons to water molecules, whereas the Lewis bases adsorbed protons from the solution. Therefore, the reported pH_{pzc} values represent the average chemistry of the carbon surface. All of the samples exhibited basic properties, which were enhanced after the cycles. In general, the larger adsorption capacity was likely related to the higher basicity of carbon, because the basic sites could adsorb SO_2 (Davini, 2002; Martin *et al*., 2002). However, the amount of SO_2 adsorbed decreased significantly along with the increase of sample basicity.

XPS was further used to investigate the chemical structure change over carbon surface. C_{1s}, O_{1s} and S_{2p} spectra were recorded for each sample, based on which the atomic ratios such as O/C and S/C were calculated and illustrated in Fig. 7. With the increase of adsorption-desorption cycles, the ascending trend for both O/C and S/C ratios was clear. Compared with original AC (A-R0), A-R10 showed a 65% increment related to S/C ratio, consistent with results of the equilibria tests that showed a sulfur loss in gas phase. Also, the higher O/C ratio after adsorption-desorption cycles gave direct evidences that more oxygen-containing species were formed.

Both the N_2 adsorption results and aforementioned FTIR results implied that pore structure and basic functional groups exhibited little effect on SO_2 adsorption and that other factors may have played more critical roles. We also observed significant increases of oxygen- and sulfur-containing species over the carbon surface after the adsorption-desorption process. Previous research has explicitly shown the negative effect of oxygen-containing species. Mochida *et al*. (1997) clarified that the surface of activated carbon fiber was most active when almost no oxygen-containing groups were present, and oxygen-containing groups were not considered to be active sites. In a subsequent paper, they attributed an

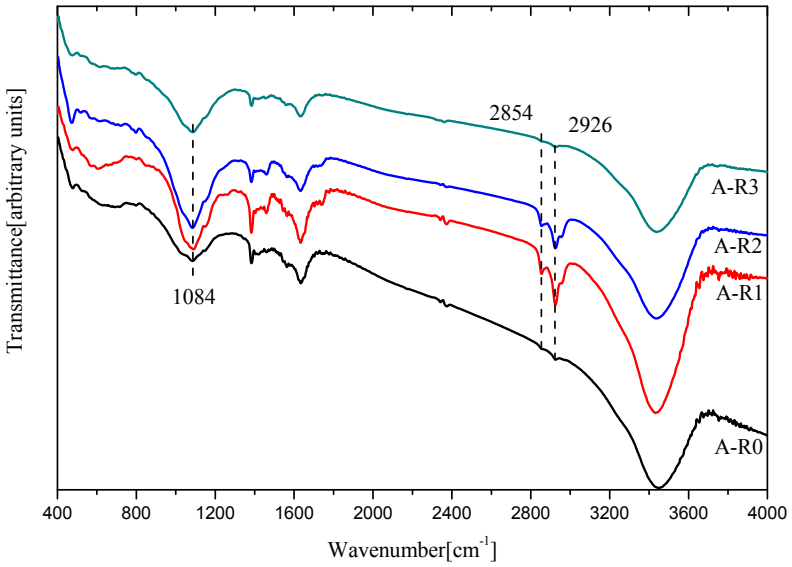

Fig. 6. FTIR spectra of the samples.

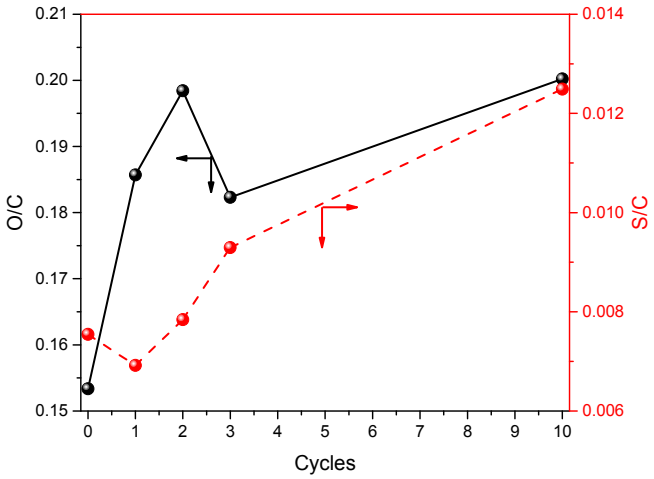

Fig. 7. O/C, S/C ratios after adsorption-desorption cycles.

increase in SO_2 adsorption capacity to an increase in the number of reactive carbon atoms, which had been generated by the evolved CO (Mochida *et al*., 1999). Lizzio and DeBarr (1996) also observed that the formation of stable C-O complexes over carbon surface occupied adsorption sites. Yang and Yang (2003) performed *ab initio* molecular orbital calculations to identify possible pathways of carbon-catalyzed oxidation of SO_2 by O_2/H_2O. Based on their theory and our findings, two deactivation pathways during the adsorption-desorption cycles were proposed, as denoted in Fig. 8. The active sites responsible for SO_2 adsorption were the zigzag edge sites with free sp^2 electrons. During the adsorption-desorption cycles, O_2 from the gas phase was involved in the formation of H_2SO_4 or SO_3, leaving one oxygen atom on the edge site to form a stable CO-forming group. This group was not removed under thermal desorption at 400°C, as indicated in Fig. 5. FTIR results also verified that the number of CO-forming groups increased after the cycles. Thus, the stable CO-forming groups may serve only to occupy the active sites, thereby inhibiting SO_2 adsorption and resulting in a significant reduction in the amount of SO_2 uptake at equilibrium.

Conversion of Ash

The original carbon contained a considerable amount of ash (15.92 wt.%), mainly composed of Si, Al, Fe, and Ca, and this ash may affect SO_2 adsorption. Table 2 presents the results of an ash composition analysis of the AC. Thermodynamic calculations at 120 and 400°C were conducted to evaluate ash conversion.

At 120°C, SO_2 reacted with Fe_2O_3 and carbon:

$$2Fe_2O_3(s) + 11C(s) + 8SO_2(g) \rightarrow 11CO_2(g) + 4FeS_2(s) \quad (3)$$

At the regeneration temperature of 400°C, H_2SO_4, Fe_2O_3, and carbon were identified as major reactants, and the complexity of the products correlated with the initial amount of H_2SO_4 (Fig. 9).

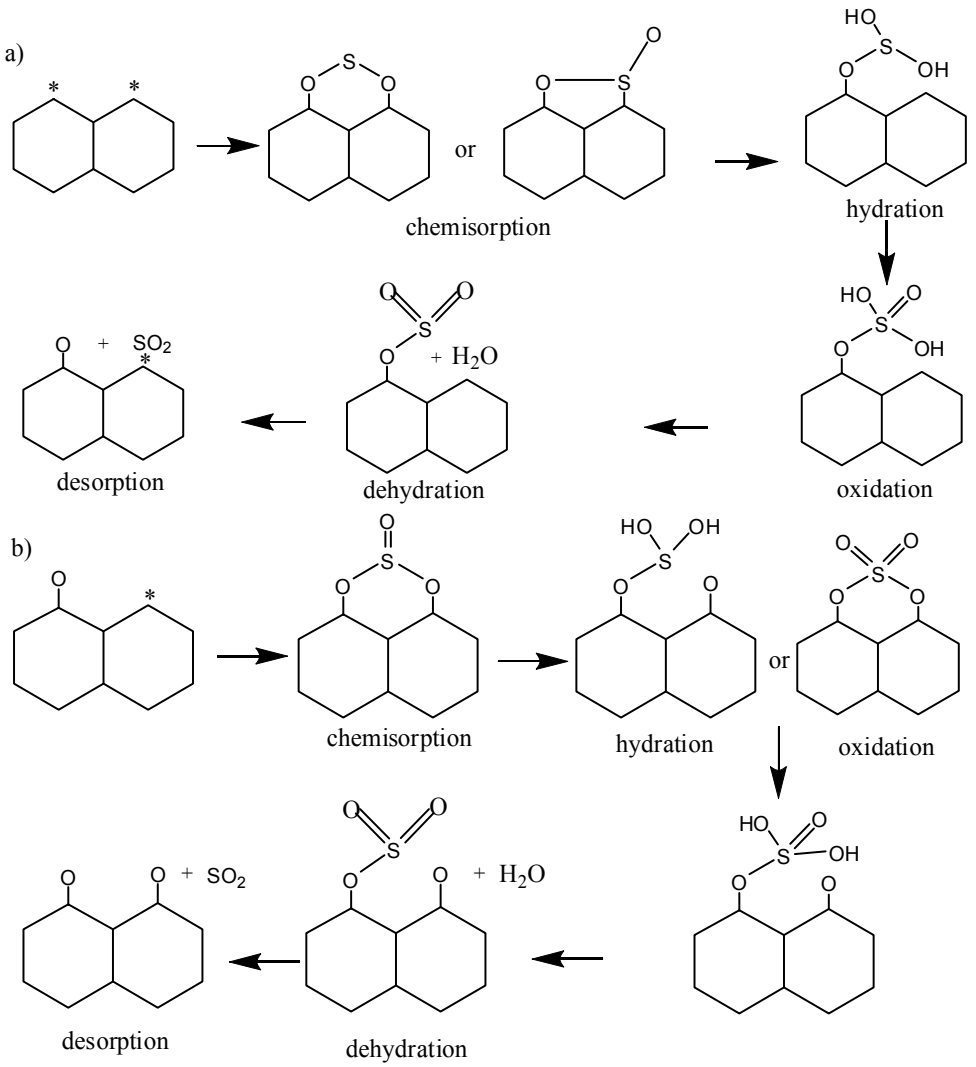

Fig. 8. Deactivation pathways of activated carbon during the adsorption-desorption cycles. (a) Without surface oxide and (b) with surface oxide; *: active sites.

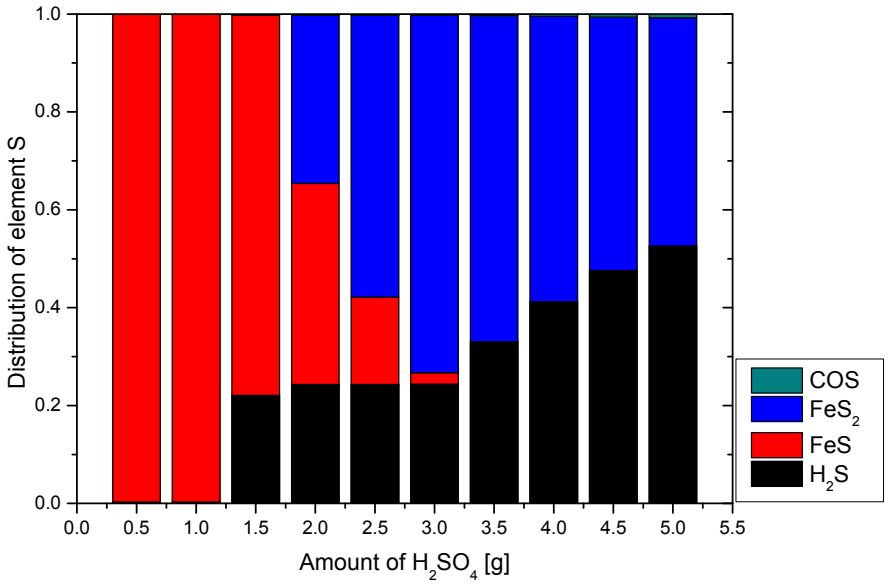

Fig. 9. Distribution of sulfur in the products.

When the amount of H_2SO_4 was below 10 mg g^{-1} AC, the H_2SO_4 reacted with Fe_2O_3 and carbon:

$$2Fe_2O_3(s) + 9C(s) + 4H_2SO_4(l) \rightarrow 9CO_2(g) + 4FeS_2(s) + 4H_2O(g) \quad (4)$$

As H_2SO_4 increased, carbon reacted with excess H_2SO_4:

$$2C(s) + H_2SO_4(l) \rightarrow 2CO_2(g) + H_2S(g) \quad (5)$$

Due to the generation of H_2S, the inert atmosphere was converted into a reduction atmosphere. With the continuous increase of H_2SO_4, some of the FeS was converted into FeS_2:

$$4FeS(s) + 6C(s) + 4H_2SO_4(l) \rightarrow 6CO_2(g) + 4FeS_2(s) + 4H_2O(g) \quad (6)$$

The reaction continued to completion until all of the Fe appeared in the form of FeS_2. These assumed reactions indicated that the SO_2 may fix on carbon as FeS or FeS_2 after the adsorption-desorption cycles. FeS and FeS_2 molecules accounted for part of the residual sulfur-containing species.

These assumed reactions were partly confirmed through X-ray diffraction (XRD) experiments (Fig. 10). All of the samples exhibited two broad peaks at approximately 2θ = 25° and 43°, corresponding with an amorphous carbon structure. In addition to these bands, XRD diffraction peaks corresponding to SiO_2 (at 2θ = 20.9°, 26.6°, 36.7°, 39.5°, and 50.1°) also appeared. A peak at 2θ = 31.4° was ascribed to Na_4SiO_4, and peaks at 2θ = 23.2° and 35.4° were caused by the presence of $CaSO_4$ crystals. Peaks at 2θ = 29.8°, 33.3°, and 38.4° were associated with FeS, FeS_2, and $FeCO_3$, respectively. These results agreed with the X-ray fluorescence (XRF) findings (Table 3), which indicated that these crystals were the major mineral components in the samples. For Sample A-R10, a strong diffraction peak was observed at 2θ = 25.4°. This peak was attributed to $Fe_2(SO_4)_3$, which was most likely the intermediate product of the reaction among H_2SO_4, Fe_2O_3, and carbon. However, amorphous $Fe_2(SO_4)_3$ may aggregate to form $Fe_2(SO_4)_3$ crystals upon heat treatment, and it can be detected using XRD. To rule out this possibility, Sample A-H10 was prepared and investigated. The XRD pattern of A-H10 was the same as that of Sample A-R0. This finding further confirmed that the $Fe_2(SO_4)_3$ crystals were a result of the reaction among H_2SO_4, Fe_2O_3, and carbon.

CONCLUSIONS

In the present study, the capacity of AC to remove SO_2 was assessed from a practical point of view. A significant reduction in the amount of SO_2 adsorbed after several adsorption-desorption cycles was observed. To determine the causes of deactivation, SO_2/CO-TPD experiments were performed. Although most of the SO_2 was released at 400°C, higher temperatures were required for the release

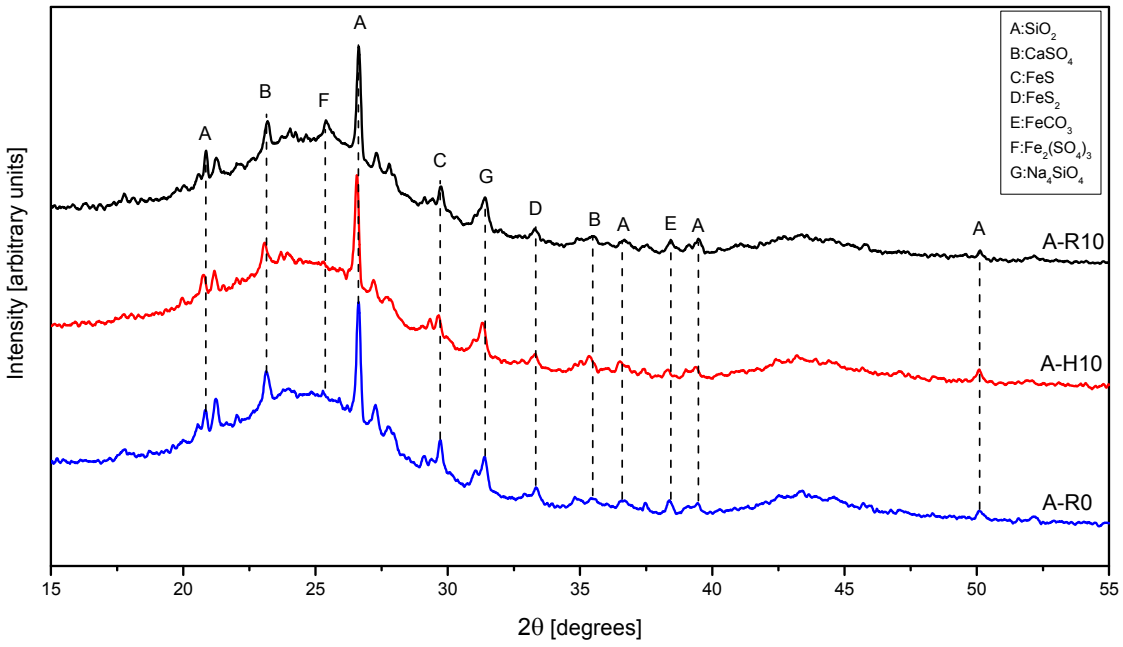

Fig. 10. XRD patterns of various samples.

Table 3. XRF characterization for AC ash.

Compound	Na_2O	MgO	Al_2O_3	SiO_2	Fe_2O_3	SO_3	CaO	F	Others
%	11.6	2.14	22.79	32.85	5.96	4.37	12.53	4.55	3.21

[a] Others: K_2O, P_2O_5, TiO_2, Cl, MnO.

of CO, and applying temperature-programmed superficial reaction theory to these results indicated that the carbon surface was oxidized after the cycles. Additionally, an FTIR experiment was conducted to investigate changes in the oxygen-containing groups, and the results confirmed the formation of stable C-O complexes, which may have occupied active sites. Based on the formation of these complexes, two deactivation pathways were proposed as being involved in the cycles. In addition to the change in oxygen-containing groups, the cycles resulted in carbon burn-off as well as subsequent changes in the physical properties of the carbon. An increase in BET surface area and a decrease in average pore size were observed. At last, the AC ash has been also changed in the cycles, during which the formation of sulfur-containing species was confirmed via thermodynamic calculation and powder XRD.

ACKNOWLEDGMENTS

This work was supported by the National Key Research and Development Program of China (No. 2017YFC0210901), the National Science Foundation of China (No. U1609212 and No. 51306079), and Open Fund of Key Laboratory of Ministry of Education of China (No. LLEUTS–201507).

DISCLAIMER

Reference to any companies or specific commercial products does not constitute.

REFERENCES

Atanes, E., Nieto-Márquez, A., Cambra, A., Ruiz-Pérez, M.C. and Fernández-Martínez, F. (2012). Adsorption of SO_2 onto waste cork powder-derived activated carbons. *Chem. Eng. J.* 211–212: 60–67.

Cui, X., Yi, H., Tang, X., Zhao, S., Yang, K., Yan, B., Li, C., Yang, X., Feng, T. and Ma, Y. (2017). Study on the properties of adsorption of SO_2-thermal regeneration cycle of activated coke modified by oxidization. *J. Chem. Technol. Biotechnol*. 93: 720–729.

Davini, P. (2001). The effect of certain metallic derivatives on the adsorption of sulphur dioxide on active carbon. *Carbon* 39: 419–424.

Davini, P. (2002). Influence of surface properties and iron addition on the SO_2 adsorption capacity of activated carbons. *Carbon* 40: 729–734.

DeBarr, J.A., Lizzio, A.A. and Daley, M.A. (1997). Adsorption of SO_2 on bituminous coal char and activated carbon fiber. *Energ. Fuel* 11: 267–271.

Gao, X., Liu, S., Zhang, Y., Luo, Z. and Cen, K. (2011a). Physicochemical properties of metal-doped activated carbons and relationship with their performance in the removal of SO_2 and NO. *J. Hazard. Mater.* 188: 58–66.

Gao, X., Liu, S., Zhang, Y., Luo, Z., Ni, M. and Cen, K. (2011b). Adsorption and reduction of NO_2 over activated carbon at low temperature. *Fuel Process. Technol.* 92: 139–146.

Gaur, V., Asthana, R. and Verma, N. (2006). Removal of SO_2 by activated carbon fibers in the presence of O_2 and H_2O. *Carbon* 44: 46–60.

Guo, Y., Li, Y., Zhu, T. and Meng, Y. (2015). Investigation of SO_2 and NO adsorption species on activated carbon and the mechanism of no promotion effect on SO_2. *Fuel* 143: 536–542.

Izquierdo, M.T., Rubio, B., Mayoral, C. and Andres, J.M. (2003). Low cost coal-based carbons for combined SO_2 and NO removal from exhaust gas. *Fuel* 82: 147–151.

Li, Y., Guo, Y., Zhu, T. and Song, D. (2016). Adsorption and desorption of SO_2, NO and chlorobenzene on activated carbon. *J. Environ. Sci.* 43: 128–135.

Liu, Q., Guan, J.S., Li, J. and Li, C. (2003a). SO_2 removal from flue gas by activated semi-cokes: 2. Effects of physical structures and chemical properties on SO_2 removal activity. *Carbon* 41: 2225–2230.

Liu, Q., Li, C. and Li, Y. (2003b). SO_2 removal from flue gas by activated semi-cokes: 1. The preparation of catalysts and determination of operating conditions. *Carbon* 41: 2217–2223.

Liu, X., Sun, F., Qu, Z., Gao, J. and Wu, S. (2016). The effect of functional groups on the SO_2 adsorption on carbon surface I: A new insight into noncovalent interaction between SO_2 molecule and acidic oxygen-containing groups. *Appl. Surf. Sci.* 369: 552–557.

Lizzio, A.A. and DeBarr, J.A. (1996). Effect of surface area and chemisorbed oxygen on the SO_2 adsorption capacity of activated char. *Fuel* 75: 1515–1522.

Ma, J., Liu, Z., Liu, S. and Zhu, Z. (2003). A regenerable Fe/AC desulfurizer for SO_2 adsorption at low temperatures. *Appl.Catal. B* 45: 301–309.

Martin, C., Perrard, A., Joly, J.P., Gaillard, F. and Delecroix, V. (2002). Dynamic adsorption on activated carbons of SO_2 traces in air I. Adsorption capacities. *Carbon* 40: 2235–2246.

Mochida, I., Korai, Y., Shirahama, M., Kawano, S., Hada, T., Seo, Y., Yoshikawa, M. and Yasutake, A. (2000). Removal of SO_x and NO_x over activated carbon fibers. *Carbon* 38: 227–239.

Mochida, I., Kuroda, K., Miyamoto, S., Sotowa, C., Korai, Y., Kawano, S., Sakanishi, K., Yasutake, A. and Yoshikawa, M. (1997). Remarkable catalytic activity of calcined pitch based activated carbon fiber for oxidative removal of SO_2 as aqueous H_2SO_4. *Energy Fuels* 11: 272–276.

Mochida, I., Miyamoto, S., Kuroda, K., Kawano, S., Yatsunami, S., Korai, Y., Yasutake, A. and Yoshikawa, M. (1999). Adsorption and adsorbed species of SO_2 during its oxidative removal over pitch-based activated carbon fibers. *Energy Fuels* 13: 369–373.

Muniz, J., Herrero, J.E. and Fuertes, A.B. (1998). Treatments to enhance the SO_2 capture by activated carbon fibres. *Appl.Catal. B* 18: 171–179.

Ni, Z.Z., Luo, K., Gao, Y., Gao, X., Fan, J.R. and Cen, K.F. (2018). Potential air quality improvements from ultralow emissions at coal-fired power plants in china. *Aerosol Air Qual. Res.* 18: 1944–1951.

Perrard, A. and Joly, J.P. (1989). A classical-model for

temperature-programmed superficial reactions. *Vacuum* 39: 551–556.

Ren, S., Guo, F.Q., Zhao, Q., Yang, J., Yao, L. and Kong, M. (2017). Sintering flue gas desulfurization with different carbon materials modified by microwave irradiation. *J. Iron. Steel Res. Int.* 24: 979–984.

Rosas, J.M., Ruiz-Rosas, R., Rodríguez-Mirasol, J. and Cordero, T. (2017). Kinetic study of SO_2 removal over lignin–based activated carbon. *Chem. Eng. J.* 307: 707–721.

Rubio, B. and Izquierdo, M.T. (1997). Influence of low-rank coal char properties on their SO_2 removal capacity from flue gases. 1. Non-activated chars. *Carbon* 35: 1005–1011.

Rubio, B. and Izquierdo, M.T. (1998). Low cost adsorbents for low temperature cleaning of flue gases. *Fuel* 77: 631–637.

Rubio, B., Izquierdo, M.T. and Mastral, A.M. (1998). Influence of low-rank coal char properties on their SO_2 removal capacity from flue gases. 2. Activated chars. *Carbon* 36: 263–268.

Shin, S., Jang, J., Yoon, S.H. and Mochida, I. (1997). A study on the effect of heat treatment on functional groups of pitch based activated carbon fiber using FTIR. *Carbon* 35: 1739–1743.

Sun, F., Gao, J., Liu, X., Tang, X. and Wu, S. (2015). A systematic investigation of SO_2 removal dynamics by coal–based activated cokes: The synergic enhancement effect of hierarchical pore configuration and gas components. *Appl. Surf. Sci.* 357: 1895–1901.

Sun, F., Gao, J., Liu, X., Yang, Y. and Wu, S. (2016). Controllable nitrogen introduction into porous carbon with porosity retaining for investigating nitrogen doping effect on SO_2 adsorption. *Chem. Eng. J.* 290: 116–124.

Wang, Y.M., Yang, X.J., Fu, P.B., Ma, L., Liu, A.L. and He, M.Y. (2017). Application of gas cyclone-liquid jet absorption separator for flue-gas desulfurization. *Aerosol Air Qual. Res.* 17: 2705–2714.

Yang, F.H. and Yang, R.T. (2003). Ab initio molecular orbital study of the mechanism of SO_2 oxidation catalyzed by carbon. *Carbon* 41: 2149–2158.

Yu, X., Liu, S., Lin, G., Zhu, X., Zhang, S., Qu, R., Zheng, C. and Gao, X. (2018). Insight into the significant roles of microstructures and functional groups on carbonaceous surfaces for acetone adsorption. *RSC Adv.* 8: 21541–21550.

Zhang, K., He, Y., Wang, Z., Huang, T., Li, Q., Kumar, S. and Cen, K. (2017). Multi-stage semi-coke activation for the removal of SO_2 and NO. *Fuel* 210: 738–747.

Zhu, Y., Gao, J., Li, Y., Sun, F., Gao, J., Wu, S. and Qin, Y. (2012). Preparation of activated carbons for SO_2 adsorption by CO_2 and steam activation. *J. Taiwan Inst. Chem. Eng.* 43: 112–119.

Received for review, July 20, 2018
Revised, September 28, 2018
Accepted, September 29, 2018